CIRA

VOLUME 31, SPRING 2009

Exploring How Improved Hurricane Forecasts Benefit Society

Colorado State University

CONTENTS

On the cover: 1948 Miami, Florida Hurricane.

(Courtesy of the National Oceanic and Atmospheric Administration/Department of Commerce)

CIRA

Cooperative Institute for Research in the Atmosphere

www.cira.colostate.edu

Editor

Laura Leinen

Design

Colorado State University, Communications and Creative Services

Technical Committee

Cliff Matsumoto, Donald Reinke, Renate Brummer, Marco Rodriguez

WRF-ARW

Evaluation and Comparison of Microphysical Algorithms in WRF-ARW Model Simulations of Atmospheric River Events Affecting the California Coast

Isidora Jankov, Jian-Wen Bao (CIRES), Paul J. Neiman (NOAA/ESRL/PSD), Paul J. Schultz (NOAA/ESRL/GSD), Huiling Yuan (CIRES) and Allen B. White (NOAA/ESRL/PSD)

Significant precipitation events in California during the winter season are often caused by land-falling "atmospheric rivers" associated with extratropical cyclones from the Pacific Ocean. Atmospheric rivers are narrow, elongated plumes of enhanced water vapor transport over the Pacific and Atlantic oceans that can extend from the tropics and subtropics into the extratropics and are easily identifiable using SSM/I polar-orbiting satellite imagery. Large values of integrated water vapor are advected within the warm sector of extratropical cyclones immediately ahead of polar cold fronts, although the source of these vapor plumes can originate in the tropics beyond the cyclone warm sector. When an atmospheric river makes a landfall on the coast of California, the northwest to southeast orientation of the Sierra Mountain chain exerts orographic forcing on the southwesterly low-level flow in the warm sector of approaching extratropical cyclones. As a result, sustained precipitation is typically enhanced and modified by the complex terrain. This has major hydrological consequences.

For the region of interest, three distinct rainfall regimes have been identified based on radar reflectivity: bright band (BB), nonbright band (NBB), and hybrid. The physical processes associated with the formation of a BB are described by House (1993 p. 198). Events that are not characterized by a BB in the radar reflectivity will be referred to as NBB rainfall. These events are associated with "shallow rain" processes in which precipitation growth is the result of condensation in low-level air that is intense enough to produce precipitation-sized raindrops before updrafts and/or orography can lift and cool the air enough to produce ice.

Previous studies that evaluated the impact that various microphysical schemes, Planetary Boundary Layer (PBL) schemes, and initial conditions had on quantitative precipitation forecasts (QPF) over the Hydrometeorological Testbed (HMT) area and for events characterized by atmospheric river settings and over the HMT area only, variations in microphysics resulted in a statistically significant impact on simulated precipitation amounts. This study builds on this finding and focuses on a detailed analysis of high-resolution numerical model forecasts of both BB and NBB events that were made using various microphysics. The simulations were performed by using the Advanced Research WRF-ARW numerical model with four different microphysics options. The evaluation consisted of comparisons of the flow and cloud structure against observations from experimental radars deployed for the HMT project.

Methodology for Microphysics Parameterization Evaluation

The model simulations were initialized at 00 UTC. The WRF-ARW model was configured with a high-resolution grid (3-km grid spacing, 32 vertical levels) covering a domain of approximately 900x600 km (Fig. 1).

The Lin, WSM6, Thompson and Schultz microphysics schemes were used in the study. All of them partition condensed water into cloud

Table 1. Observed total precipitation in millimeters, and the precipitation type classification at the two S-band radar locations, Cazadero (CZD) and Alta (ATA). BB, NBB, and Mixed stand for brightband, nonbrightband and mixed precipitation regimes expressed in storm-total percentages, respectively. '——' represents missing data.

Locations	Atmospheric River Events				
Fcst. Init. 00 UTC	30 Dec05	01 Jan06	01 Feb06	27 Feb06	05 Mar06
Fcst. Length (hr)	48	36	42	36	36
Precip. Amount (mm)	CZD: 208.0 ATA: 229.4	CZD: 90.7 ATA: ——	CZD: 47.2 ATA: 56.5	CZD: 161.8 ATA: 82.5	CZD: 124.4 ATA: 75.5
Precip. Type (%BB/%NBB)	CZD: 75/18 ATA: 90/7	CZD: 7/85 ATA: 93/7	CZD: 16/80 ATA: 38/62	CZD: 48/39 ATA: 74/20	CZD: 90/8 ATA: 100/0
Dominant Precip. Type	CZD: BB ATA: BB	CZD: NBB ATA: BB	CZD: NBB ATA: NBB	CZD: Mixed ATA: BB	CZD: BB ATA: BB

WRF-ARW

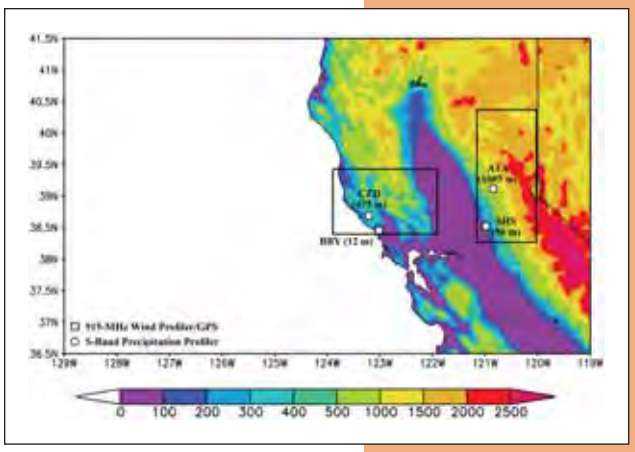

Figure 1. Integration domain and terrain base map of Northern California, with the wind profiler sites shown at Bodega Bay (BBY) and Sloughhouse (SHS), and the S-band radar sites shown at Cazadero (CZD) and Alta (ATA). The terrain height is expressed in meters and x and y axes represent longitude and latitude of the area, respectively. The largest box represents the area of water species integration while the two smaller boxes indicate areas used for average rain, mean absolute error (MAE) and equitable threat score (ETS) calculations.

liquid, cloud ice, rain, snow, and graupel (precipitation which forms when enough supercooled droplets of water condense on a snowflake to increase the snowflake's fall speed). For each of the four microphysics configurations, the nonlocal mixing Yonsei University (YSU) PBL scheme (Noh et al. 2003) – as an improved version of the Medium-range Forecast Model (MRF) PBL scheme (Troen and Mahrt 1986) – was used. The analyses of the results were based on the model hourly output.

Relevant mesoscale attributes for each of the five storms were evaluated based on observations from 915-MHz wind profilers, vertically pointing S-band radars and collocated GPS water-vapor sensors, and surface meteorological instrumentation in two key domains: the coastal region northwest of San Francisco and the interior region east of Sacramento (Fig. 1). The instrumentation in the coastal region included a wind profiler and GPS device on the coast at Bodega Bay (BBY – 12-m MSL) and S-band radar in the coastal mountains at Cazadero (CZD – 475-m MSL). The interior region featured a wind profiler and GPS in the Central Valley at Sloughhouse (SHS – 50-m MSL) and S-band radar in the Sierra foothills at Alta (ATA – 1085-m MSL). Finally, all sites were equipped with tipping-bucket rain gauges and towers that recorded standard meteorological surface data every two minutes.

The S-band radar data at the two locations were used to classify the five events into the BB and NBB precipitation regimes and to evaluate the model's ability to discriminate between the two regimes. In this approach particles are assumed to be spheres with constant density, with different densities for raindrops, snow flakes, and graupel. The size distribution follows the exponential function and the intercept parameter is assumed to be constant. In addition, the synthetic radar imagery package includes the adjust factor for BB, where snow and graupel particles scatter like liquid water if it is assumed they have a liquid skin (melting process started). The utilization of the synthetic reflectivity estimation for various model configurations allows for a direct comparison of results.

Observational Analysis and Model Simulations of the Representative Atmospheric River Events

The five events under consideration were associated with atmospheric rivers making landfall in California. Although all five storms were investigated, only two of them (30 December 2005 and 01 February 2006) will be the focus of discussion for the sake of conciseness. The December storm was classified as a BB event at both CZD and ATA, while the opposite was true for the February storm.

(a) 30 December 2005 Event

The strongest event of the five cases studied occurred on 30 December 2005 when >200mm of rain fell in the mountainous terrain at each S-band radar site. A time-height section of hourly wind profiles and along-front isotachs along the coast at BBY (Fig. 2a) shows the temporal descent of warm-frontal shear (highlighted by a descending axis of thermal-wind-derived warm advection) from ~3 km MSL at 22 UTC 29 December to near the surface at 16 UTC 30 December, followed by enhanced southwesterly flow and multiple low-level jets (LLJs) in the warm sector. Concurrent S-band radar observations at CZD (Fig. 2b) documented mostly NBB rain during the warm-frontal descent and a mix of NBB and BB rain in the warm sector. The integrated water vapor (IWV) at BBY attained its maximum values (2.5 to 3.5 cm; Fig. 2c) in the strong warm-sector flow, indicative of atmospheric-river conditions. Because the along-front isotachs in this case approximately represent the incoming flow orthogonal to the mean orientation of the mountain barrier (i.e., upslope flow), and the strongest upslope flow coincided with the heaviest rain in the downstream mountains at CZD (Fig. 2c), it

is likely that orographic processes enhanced the rainfall intensity. A descending zone of cooling aloft was inferred by the BBY profiler starting at ~13 UTC 31 December, as evidenced by the commencement and subsequent descent of thermal-wind-derived cold advection and an abrupt decrease in IWV and rain intensity. A model-derived time-height section of equivalent potential temperature from BBY (not shown) captured this forward-tilted feature, as did the 850- and 700-mb analyses at 1200 UTC 31 December (also not shown). Four hours later, a robust, surface-based cold front accompanied by a 3-km-deep wind shift from southwesterly to northwesterly flow crossed the profiler. A brief spike in precipitation and a second stepwise decrease in IWV were observed with this front. The precipitation immediately preceding the cold frontal passage, which represented a period of enhanced and deep mesoscale forcing, exhibited the strongest BB characteristics during the event.

Corresponding time-height sections of hourly wind profiles and along-front isotachs at BBY simulated by the model run using Lin microphysics showed that all major mesoscale features were generally depicted by the model (Fig. 3). The temporal descent of the warm-frontal shear had the right timing and was followed by enhanced southwesterly flow and multiple LLJs within the warm sector. Even though the LLJs were depicted by the model, not all of them had a good timing and correct vertical distribution of momentum. With regard to simulated IWV at BBY, the maximum value (2.5 to 3.8 cm; not shown) was simulated within the strong warm-sector flow. This agreed well with the observations except that the peak value was slightly overestimated. The maximal values of simulated IWV were consistent among various model configurations. As in the analysis, the maximum in simulated precipitation generally coincided with the maximum in simulated upslope flow (Fig. 3b), but all model versions were characterized with the extended precipitation longevity and higher simulated amounts compared to the analysis. This may be related to the fact that simulated moisture content as well as wind upslope component intensity and duration were somewhat overestimated by all model versions. Finally, the cold-frontal passage aloft was relatively well depicted by the model, except that the flow intensity was once again overestimated. At the surface, the model was too slow with the trough passage. During the 16 to 23 UTC period on 31 December, low-level flow shifted from southwesterly to westerly but not to northwesterly as observed.

This event was also well documented along the windward slope of the Sierras at SHS and ATA (not shown), although the meteorological transitions here were not nearly as well-defined as along the coast. The model simulation of the flow at SHS generally captured all major features well (not shown). Precipitation and radar reflectivity simulated from the different model versions will be discussed later.

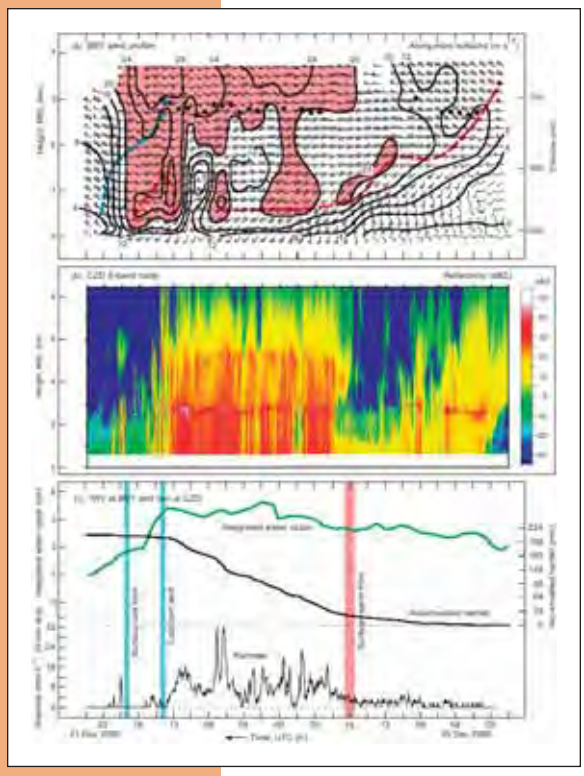

Figure 2. Time series of observations from BBY and CZD between 22 UTC 29 December and 22 UTC 31 December 2005. a) Time-height section of hourly-averaged wind profiles (wind flags 25 m s^{-1}; barbs = 5 m s^{-1}; half-barbs = 2.5 m s^{-1}), along-front isotachs (directed from 230°; red shading >20 m s^{-1}), bright band melting-level height (bold black dots), and axes of maximum thermal wind-derived warm and cold advection (red and blue dashed lines, respectively), from the wind profiler at BBY. b) Time-height section of ~1.5-min radar reflectivity (dBZ) from the S-band radar at CZD. c) Time-series traces of 30-min IWV (cm; green) from the GPS sensor at BBY and 2-min rain accumulation (mm) and rain rate (RR = mm h^{-1}; 10-min averaging period) data recorded at the rain gauge at CZD. The red- and blue-shaded bars in the bottom panel denote warm- and cold-frontal transitions, respectively.

(b) 01 February 2006 Event

Compared to all other cases evaluated in this study, the event of 01 February 2006 possessed the weakest winds, the least distinct transient meteorological features, and the lightest precipitation accumulation (~50 mm) of the five events. At BBY, moderate westerly to southwesterly flow on the warm side of a warm front descended from ~1.5 km MSL to the surface between 06 and 13 UTC 1 February. The rain at CZD was primarily NBB in character, except for a short period of BB rain near 16 UTC 01 February. Also, rainfall at CZD commenced as the low-level upslope flow increased to >8 m s-1 and the IWV at BBY increased steadily (to values eventually exceeding 3 cm) on the warm side of the descending warm front (not shown). An LLJ was conspicuously absent in the warm sector, where the flow oscillated between southwesterly and west-northwesterly. After ~1130 UTC 02 February, the

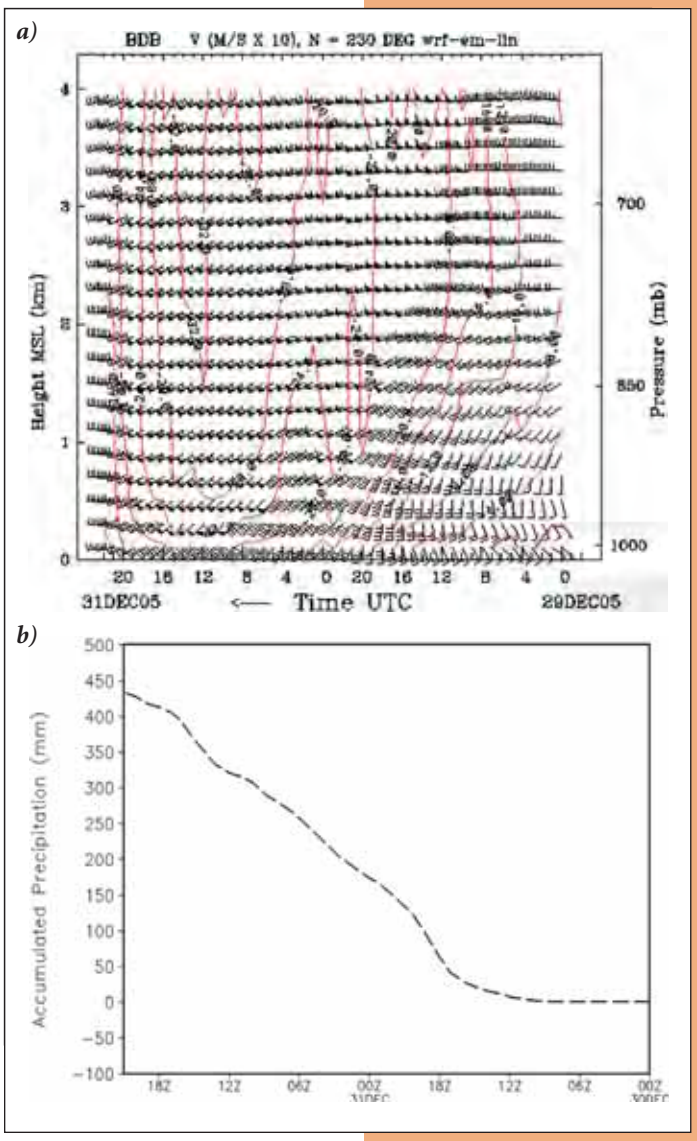

Figure 3. Simulated a) wind profile at BBY and b) precipitation accumulation by the model run using Lin microphysics for the period 00 UTC 30 December to 22 UTC 31 December 2005. Wind flags, barbs, and isotachs are as in Fig. 2.

low-level winds slowly veered with time from west-southwesterly to northwesterly, the IWV decreased from ~3.0 to 2.3 cm, and the rainfall ended, all in response to a weak cold-frontal passage. The sequence of events was generally similar in the interior (not shown), except that the cold-frontal wind shift started aloft a couple of hours later (~15 UTC 02 February at SHS) and was unable to penetrate downward through the low-level, 1-km-deep blocked flow. The S-band radar at ATA documented alternating periods of NBB and BB rain (62% and 38% of the total, respectively).

At BBY, timing of the moderate westerly to southwesterly flow descent from ~1.5 km MSL to the surface on the warm side of a warm front was generally well depicted by the model using Lin microphysics (not shown). Simulated low-level flow on the warm side of the descending warm front also increased to values > 8 ms-1, but the model was somewhat slow in shifting winds from southwesterly to westerly at the precipitation initial time (not shown). This likely caused precipitation initiation delay of ~7 hrs for all model configurations compared to observations. With regard to simulated precipitation amounts, different model versions resulted in different simulated amounts, but all of them were characterized by a notable overestimation. Simulated IWV, of ~3.4 cm, was higher than observed (not shown). Consequently, high precipitation amounts and extended longevity may be once again related to the model's overestimation of moisture content and both intensity and duration of the enhanced upslope wind component. Precipitation simulated by different model versions will be discussed in more detail later in the text. Similarly at SHS, the intensity of the upslope flow component was slightly overestimated (not shown). Simulated precipitation started ~8h earlier compared to observations and all model solutions resulted in much larger rain rates than observed. At this location, simulated reflectivity from all model versions consisted mainly of NBB.

Microphysical Aspects of the Model's Performance

(a) Water Substance Partitioning

The microphysics schemes used in this study partition water condensate into cloud liquid, cloud ice, rain, snow, and an additional category for precipitating ice that falls significantly faster than snow. This is usually called graupel, but it is used to represent frozen rain (sleet), compacted aggregates of snow crystals, rimed snow crystals, and all types of hail. Unfortunately, this variety of hydrometeors can only be dynamically represented by a single function expressing the precipitation sedimentation rate as it relates to the condensate mixing ratio. This is unfortunate because there is tremendous variability in fall speed among the various types of precipitating ice in nature. Other modeled microphysical processes are also affected by ice habit, such as latent heat release rate (associated with deposition, sublimation, melting, and riming) and conversions among the categories by collection. Choices made about ice process parameters in the microphysics schemes must be made based on the expected dominant type of precipitating ice, and these choices can cause large variations in forecast results. It is beyond the scope of this

study to isolate and quantify the effects of parameter variations, but it is useful to consider certain aspects of their collective results to understand their impacts on forecasts of precipitation and synthetic reflectivity.

One simple but informative diagnostic is the volume-integrated water mass by the microphysical species. This diagnostic was evaluated over the area indicated by the largest of the three boxes in Fig. 1. Figure 4 shows the average mixing ratios of cloud water, cloud ice, rain, snow, and graupel for four different microphysical schemes; the averages were computed over all five cases. It can be seen that in the Lin scheme, cloud water dominated over cloud ice, and rain and graupel dominated over snow. Results of water substance partitioning for the WSM6 scheme appeared to be very similar to the results obtained with the Lin scheme; note however, that these two schemes were characterized with much larger graupel presence compared with the other two schemes. In the Thompson scheme, the dominance of cloud water over cloud ice was even more distinct when compared with the Lin and WSM6 schemes; rain and snow dominated over graupel. In addition, the Thompson scheme was characterized with the largest values of rain and snow mixing ratios compared to all other schemes. This was especially true for the snow mixing ratio. Contrary to all the other schemes, the Schultz scheme was characterized with much more cloud ice compared to cloud water. Snow and rain were also equally present in this scheme. The graupel mixing ratio was much smaller compared with mixing ratios of other hydrometeors, as well as compared with the graupel mixing ratios of the Lin and WSM6 microphysics.

Overall, cloud matter (sum of cloud ice and cloud water) was generally equally present in all the schemes. In terms of hydrometeors, the same was valid for rain. Snow was notably more present in the Thompson and Schultz schemes compared with the Lin and WSM6 schemes, while the opposite was true for graupel. The implications of these results are incorporated into discussions below on the model's performance.

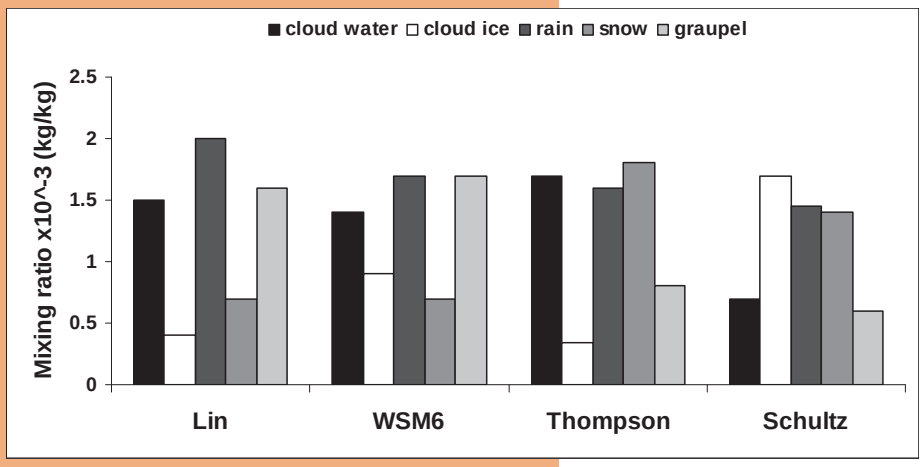

Figure 4. Cloud water, cloud ice, rain, snow and graupel mixing ratios ($\times 10^{-3}$ kg/kg) averaged over five cases and over the American River Basin for four different microphysics schemes.

(b) Precipitation Simulations from Four Different Model Configurations

At CZD, two out of five cases were classified as BB, two were classified as NBB precipitation events, and one event was characterized as a mix of precipitation regimes (BB and NBB types were equally present in terms of storm-total percentages). This classification was different at ATA. The ATA location was characterized with a BB precipitation type for four out of the five events. To validate simulated precipitation accumulations, rain gauge data at these two locations were used.

At CZD, for both events classified as BB and NBB, all model versions almost always resulted in a notable overestimation of simulated precipitation amounts (not shown). For the BB events, accumulated precipitation amounts simulated by Lin, WSM6, Thompson, and Schultz schemes were on average overestimated by 102%, 72%, 73% and 42%, respectively. For the cases classified as NBB (Figs. 5b and c), the overestimation was notably reduced compared to the BB events. Expressed in percentages, it was 42%, 42%, 21%, and 11% for the model runs using the Lin, WSM6, Thompson, and Schultz microphysics schemes, respectively.

At ATA, the situation was similar. All model runs were characterized by a remarkable overestimation of accumulated precipitation amounts (not shown). At this location four out of the five events were classified as BB. For these four, or more precisely three events (for the

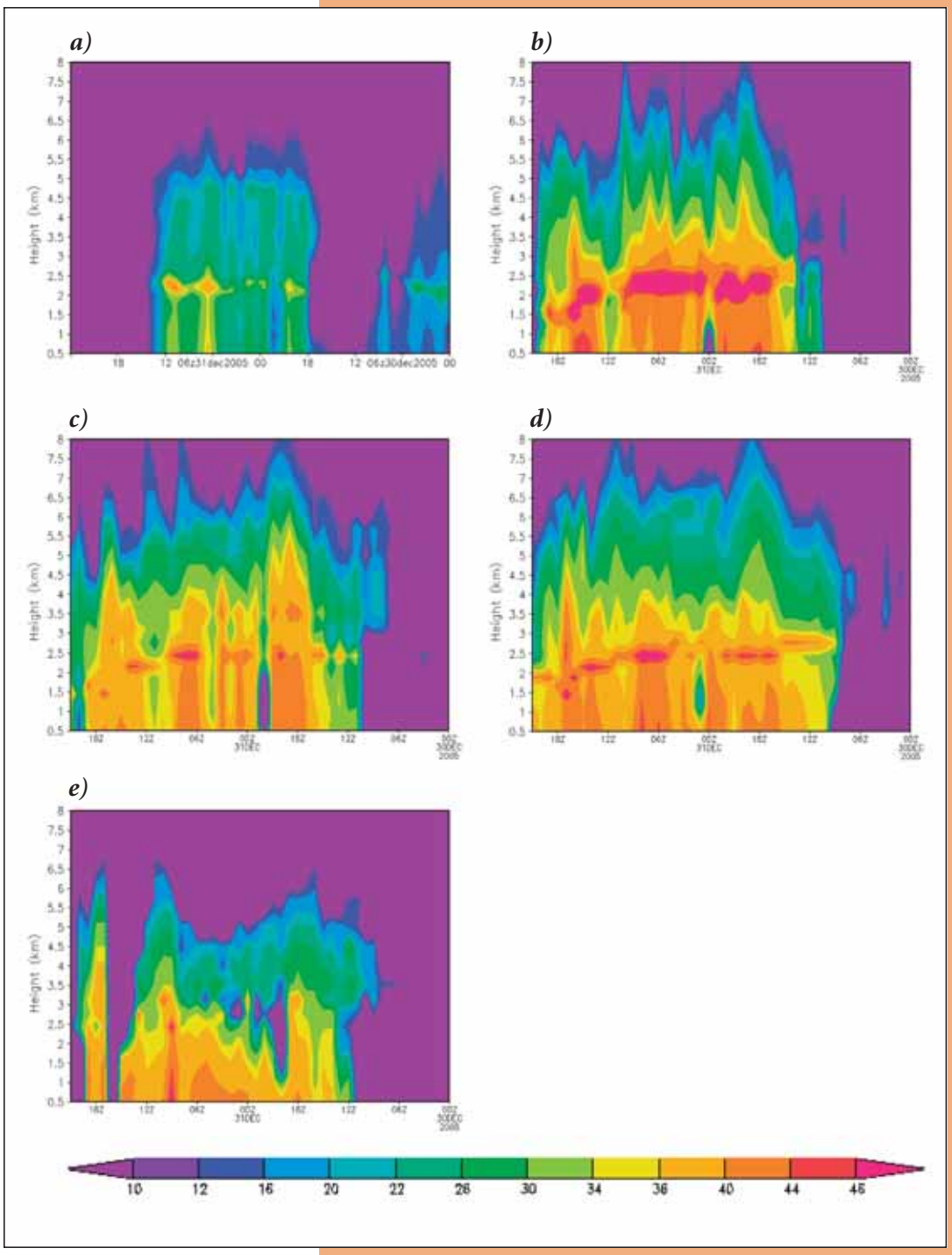

Figure 5. Hourly radar reflectivity (dBZ) at CZD: a) observed, and simulated with b) Lin, c) WSM6, d) Thompson and e) Schultz microphysics for a 48-hour period starting at 00 UTC 30 December 2005.

01 January 2006 case observations were missing), overestimations on average were 108%, 100%, 48%, 47%, for model runs using Lin, WSM6, Thompson, and Schultz schemes, respectively. In the case of one NBB event, the overestimations for different model runs were 47%, 100%, 100%, 45%.

Overall, for both BB and NBB events at the two locations, all schemes almost always resulted in a large overestimation of accumulated precipitation amounts, which is possibly related to the earlier discussed overestimation of the intensity and duration of the upslope wind component as well as to a slight overestimation of the moisture content. However, a large difference in simulated amounts among model runs using various microphysics was detected.

(c) Comparison of Synthetic Versus Observed Radar Reflectivity

Synthetic reflectivity from the four different model microphysics schemes was compared to the observed reflectivity data obtained from the vertically pointing S-band radars at CZD and ATA. To match the model's 1-h-resolution output, the observed S-band, 2-min radar reflectivity data were averaged into 1-h blocks. Synthetic versus observed radar reflectivity was compared using the four model microphysics configurations for all five cases, but for the sake of conciseness, only the results from two key cases: the BB event of 30-31 December 2005 and the NBB event of 01-02 February 2006 will be discussed in detail.

(1) 30-31 DECEMBER 2005 CASE

Figure 6 shows hourly observed reflectivity values and synthetic reflectivity from the four model configurations at CZD for a 48-hour period starting at 00 UTC 30 December 2005. During the warm-frontal shear period (between ~22 UTC 29 December 2005 and ~16 UTC on 30

December 2005), observed reflectivity documented mostly NBB rain with a maximum value of ~30 dBZ (Fig. 5a). The warm sector period was characterized by a mix of NBB and BB rain. The BB height was at ~3km and the maximum in BB reflectivity of ~45 dBZ was detected immediately preceding a cold- frontal passage.

Figures 6b-e show that all model versions missed precipitation during the first six simulation hours. This is consistent with a slight delay in precipitation initiation and an underestimation of the simulated rain rate by all model configurations. With regard to the period of mixed NBB and BB precipitation, results differ among various simulations, but in all of them, the BB and precipitation persisted longer than observed, a period between 12-18 UTC on 31 December 2005. This agreed well with an overestimation of precipitation longevity, discussed earlier. In addition, all simulations resulted in a general reflectivity intensity overestimation. With regard to the simulation of the BB reflectivity feature, the model runs using the Lin, WSM6, and Thompson schemes resulted in a well-defined BB, but its intensity was largely overestimated (Fig. 5b, c, and d). This was especially true for the model run using the Lin scheme. Furthermore, this model run was characterized by a large BB depth overestimation. The model run using the Schultz scheme was generally characterized by a moderate reflectivity overestimation compared to observations, but the BB was not well defined in that case.

Differences in the synthetic reflectivity between various model versions were further assessed by analyzing plots of simulated snow, rain, and graupel mixing ratios with simulated 0°C temperature and wetbulb temperature lines included (Fig. 6). OAK soundings are plotted as asterisks. For all model versions, the 0°C temperature and wetbulb temperature lines overlap for most of the simulation period, indicating saturated conditions. The 0°C-level heights were almost identical for all model versions and generally in good agreement with available observations. It is noteworthy that model runs using the Lin and WSM6 microphysics were characterized by a layer only graupel mixing ratio in (Figs. 7a and b). In this layer, both the Lin and WSM6 microphysics virtually converted all snow into graupel. The layer containing pure graupel was deeper for the model run using the Lin scheme, which likely resulted in, the larger BB depth, as discussed earlier. At ATA this event was also classified as a BB event. Synthetic reflectivity and simulated mixing ratio images indicated similar behavior among the schemes as at CZD (not shown).

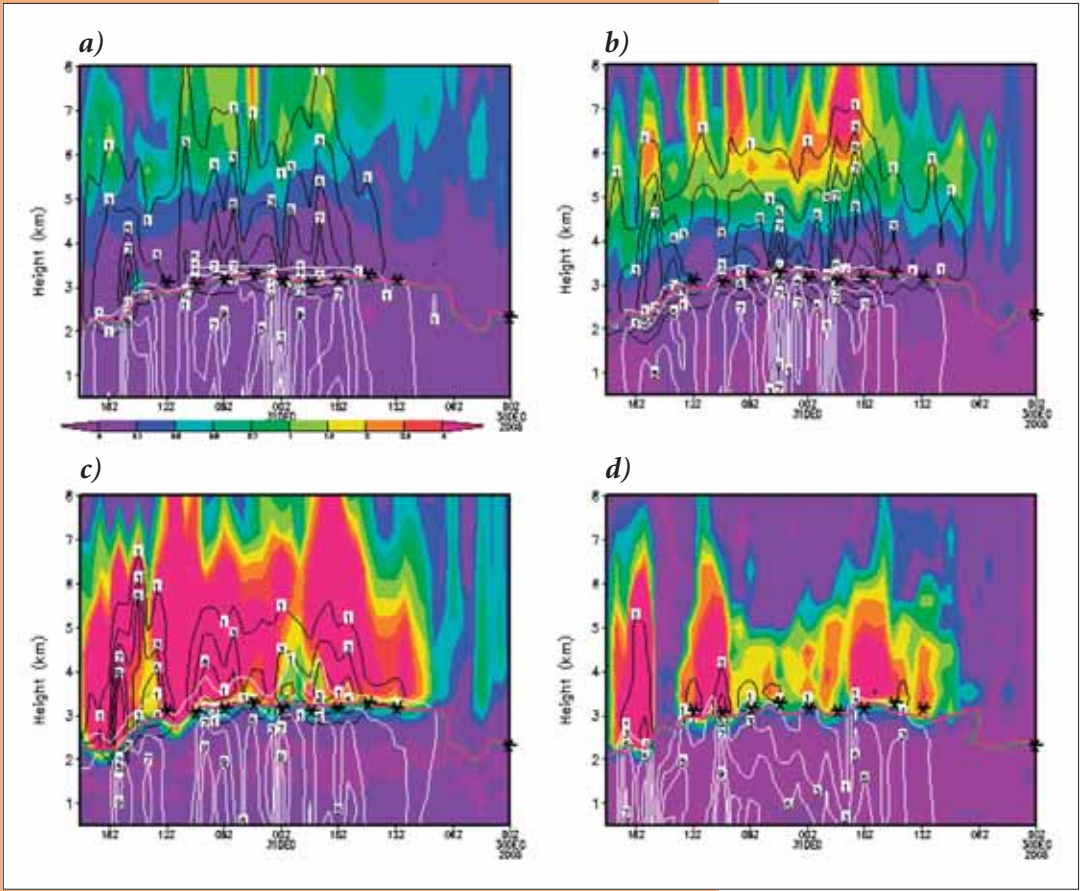

Figure 6. Snow (color shaded, see color bar), rain (white contours), and graupel (black contours) mixing ratios (kg/kg), and 0°C temperature (red) and wetbulb temperature (green) lines for the December 30, 2005 case at CZD for model runs using a) Lin, b) WSM6, c) Thompson, and d) Schultz microphysics. Melting level heights, shown as '', from available OAK soundings. Both shading and contours are scaled by a factor of 10^{-4}.*

WRF-ARW

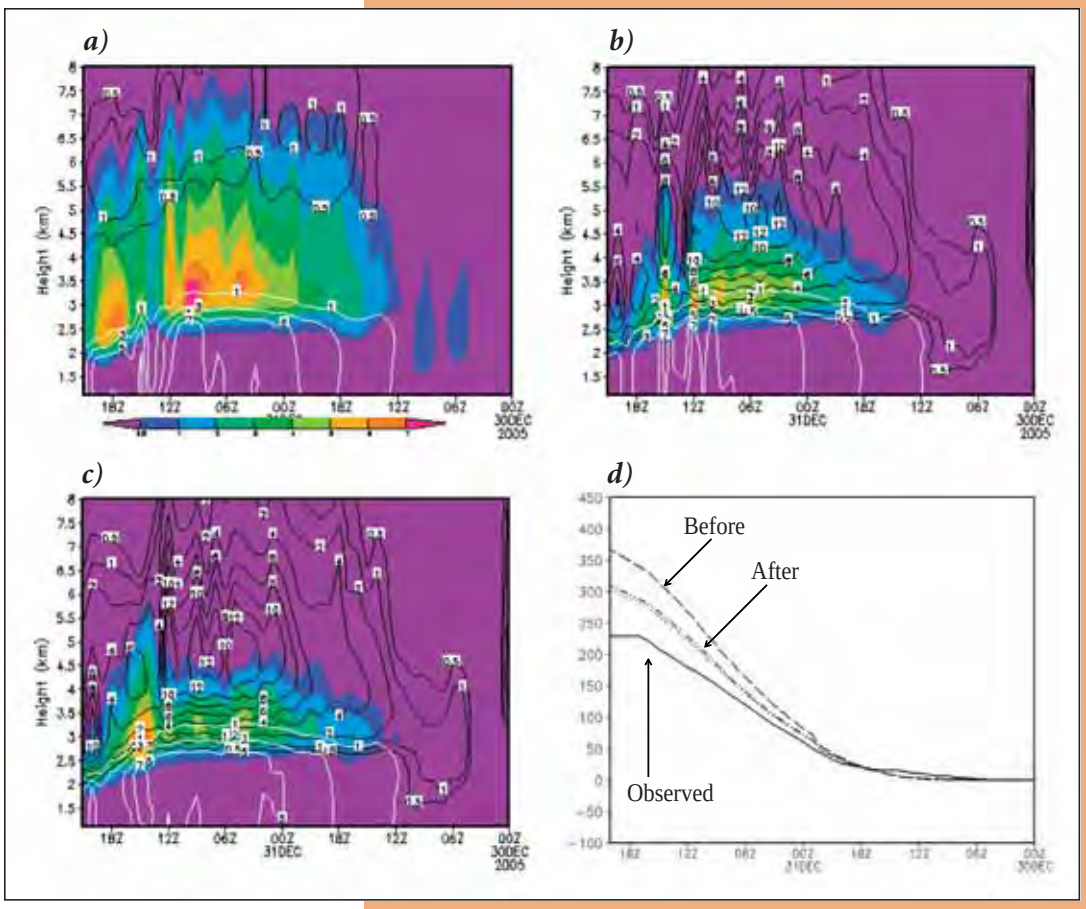

Figure 7. Time-height presentation of snow (black contours), graupel (color shaded), and rain (green contours) mixing ratios (kg/kg) for the ATA 30-31 December 2005 case for a) the model run using unchanged Lin microphysics, b) the model run using Lin microphysics with the snow accretion by graupel set to zero and c) the model run in which the accretion of snow by graupel was set to zero and the threshold for autoconversion of snow by graupel was lowered. Both shading and contours are scaled by a factor of 10^{-4}. The impact of the two experiments on 48-hour simulated precipitation accumulations is presented in panel d.

(2) 01-02 FEBRUARY 2006 CASE

At both CZD and ATA, the 01 February 2006 case was classified as a NBB precipitation event. Overall, the synthetic reflectivity values were overestimated by all model configurations (not shown). The reflectivity overestimation in the melting layer region pointed to BB presence for model runs using the Lin, WSM6, and Thompson schemes when no BB was observed. Simulated snow, rain, and graupel mixing ratios indicated the same behavior as in the case of the BB event (not shown). In terms of 0°C-level height, it was once again reasonably well simulated by all model configurations compared to available soundings. A cloud layer much deeper than observed was common among all the model configurations. This was consistent with the model's overestimation of the moisture flux intensity and duration.

(d) Sensitivity Tests

Two characteristics of the model runs using the Lin and WSM6 schemes were noted. First, almost all the frozen condensate was quickly converted to the graupel category. Second, the precipitation amounts were often greater for these schemes than for the others and for all locations. This was especially true for cases classified as BB events, cases dominated by ice processes. We hypothesize that the precipitation excess is related to the scheme's aggressive graupel formulations, because graupel falls much faster than snow or cloud ice, allowing less time for evaporation as it falls. Also, there would be less evaporation of precipitation because graupel evaporates more slowly than an equivalent mass of snow, which has a far greater surface area.

Two experiments involving the Lin scheme were performed to test this hypothesis, and the results are presented in Fig. 7. In the first experiment, accretion of snow by graupel was set to zero. The results showed that an elimination of this process produced notably less graupel (Fig. 7b). The previously discussed deep layer containing only graupel was no longer present. In the second experiment, in addition to setting the accretion of snow by graupel to zero, the autoconversion of the snow to graupel threshold was lowered. Lowering the autoconversion threshold further decreased graupel production but not considerably (Fig. 7c). In terms of simulated precipitation amounts, disregarding the accretion process reduced the precipitation overestimation for ~50%, while the positive impact of a lowered autoconversion threshold was negligible (Fig. 7d).

These results suggest a possible adjustment of the microphysical schemes' performance for specific types of meteorological scenarios. These

types of adjustments may help improve QPF by reducing bias associated with microphysical parameterizations, but they cannot help with the bias caused by errors in the larger-scale flow.

Summary

The main goal of the present study was to evaluate the performance of a high-resolution, numerical model using four different microphysics schemes for five significant precipitation events during a winter season in California associated with atmospheric river settings. In addition, these cases were chosen to examine the models' ability to discriminate bright band (BB) from nonbright band (NBB) precipitation regimes. Simulations of the five atmospheric river events were performed using 3-km grid spacing in the WRF-ARW model and four different microphysical options: Lin, WSM6, Thompson, and Schultz. Eta model forecasts were used for specifying initial and lateral boundary conditions. The evaluation involved comparisons of the flow and cloud structure against special observations from the HMT project. The models' ability to depict relevant mesoscale attributes was evaluated against the 915-MHz wind profiler. S-band radar reflectivity data were used for classification of the assessed events to BB and NBB categories and to evaluate the model's ability to discriminate between the two precipitation regimes. Tipping-bucket rain gauges were used for verification of simulated precipitation accumulations.

The analyses of hourly vertical wind profiles showed that the model represented the basic synoptic-scale flow reasonably well without introducing much apparent nonphysical detail, and produced reasonable mesoscale features, some of which were validated with observations. The model also showed a tendency to overestimate the upslope wind component duration and intensity as well as moisture content. This is probably an artifact of a small sample size (5) and not indicative of any symptomatic bias.

Water substance partitioning results indicated a similarity between the Lin and WSM6 microphysics, characterized by much more cloud water compared to cloud ice and more rain than snow. More importantly, the graupel mixing ratio content for the two schemes was notably larger than in the Thompson and Schultz microphysics. The largest snow mixing ratio and the smallest graupel mixing ratio values were detected for the Thompson and Schultz schemes, respectively. Whereas the Lin and WSM6 schemes can be expected to perform similarly given the history of their origins, the Thompson and Schultz approaches have no such overlap.

In essence, simulated precipitation amounts for atmospheric river events revealed a large sensitivity to the choice of microphysics, verifying location, and precipitation regime (BB vs. NBB); the model's errors in the larger-scale flow had an impact as well. The same was true for synthetic reflectivity. Differences in performance among various microphysical schemes were largely attributed to variations in the partitioning of water substance. Based on these results, a hypothesis related to the model performance for BB events was established. Testing of the hypothesis involved altering certain parameters within various microphysical schemes and evaluating the impact of these changes on the schemes' behavior and consequently on the simulated precipitation. Future studies should focus on improving nonconvective precipitation accuracy by objectively estimating the individual contributions of those parameterized processes that represent generation and depletion of various hydrometeors. This is expected to lead to methods for objectively adjusting critical parameters in microphysics schemes, and consequently to precipitation prediction improvement.

CUMULUS CLOUDS

Effect of Aerosol and Model Resolution on Small Cumulus Clouds

Hongli Jiang and Graham Feingold

Introduction

Photographs of cumulus clouds taken from high-flying aircraft (*Plank*, 1969) reveal that cumulus clouds have sizes ranging from 30 m to 10 km. Satellite imagery from Landsat (30 m resolution) and ASTER (15 m resolution) indicate the existence of small clouds down to the instrument detection limit. Because small clouds exist in much higher numbers than large clouds, they have been found to dominate mass flux transport, contributions to cloud fraction, and possibly to cloud reflectance. Given their importance, it is of interest to consider their response to aerosol perturbations and how this response varies with grid resolution.

Cumulus clouds exhibit a great deal of variability in size and depth. There is considerable disagreement about their response to aerosol. The change of cloud fraction cf in response to an increase in aerosol concentration N_a can be either greater or less than zero. The sign of the change in liquid water path (LWP) in response to aerosol changes may or may not have the same sign as cloud fraction responses, in contrast to typical assumptions that an increase in aerosol will reduce the ability of a cloud to precipitate, increase cloud liquid water, and extend cloud coverage (the "second indirect effect" of aerosol on clouds).

Given these uncertainties, the study of *Jiang et al.* 2009 has evaluated aerosol effects on the microphysical, macrophysical, and radiative properties of a population of shallow cumulus generated by a large-eddy model. We present some highlights from that study below.

Model and Case Description

We use a model to assess the sensitivity of cumulus cloud properties to aerosol changes at a range of model resolutions. The model is an adaption of the Regional Atmospheric Modeling System (RAMS version 6.0) coupled to a microphysical model which includes a size-resolving representation of cloud and raindrops (Feingold et al., 1996). The thermodynamic sounding taken from the Rain In Cumulus over the Ocean (RICO) field experiment (*Rauber et al.*, 2007) is used for all the simulations. We tested this case under assumed clean aerosol conditions (N_a = 100 cm^{-3}) and polluted conditions (N_a = 1000 cm^{-3}). The horizontal model grid is varied from $\Delta_{x,y}$ = 100 m to $\Delta_{x,y}$ = 25 m and the vertical grid from Δ_z = 40 m to Δ_z = 10 m.

Cloud Size Distribution, *n(a)*

The cloud size distribution *n(a)* of a cumulus population is defined as the number of occurrences of clouds per area range *a*. Cloud fraction can be derived from the first moment of cloud size distribution, and the total reflectance can be approximated as the product of the first moment of cloud size distribution and the two-stream approximation of nadir reflectance (a function of cloud optical depth τ_c). As can be seen in Figure 1a, the cloud size distribution follows a negative power-law distribution, and polluted cloud fields are characterized by more

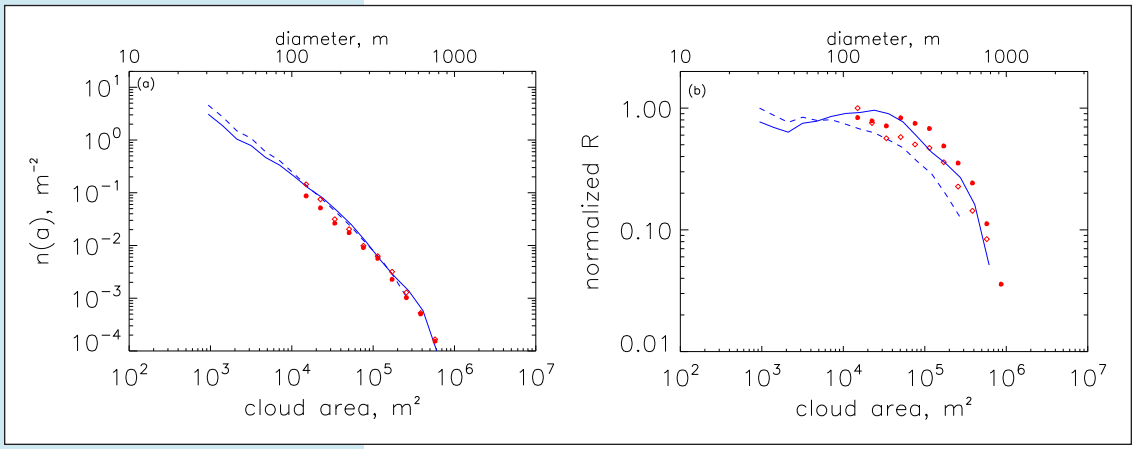

Figure 1. (a) Cloud size distribution* n(a) *with respect to cloud area* a*, and (b) normalized total reflectance* R*. The cloud diameter (the square-root of* a*) is labeled at top. Lines denote the fine resolution ($\Delta_{x,y}$ = 25 m, Δ_z = 10 m,), and symbols represent the coarse resolution ($\Delta_{x,y}$ = 100 m, Δ_z = 40 m,). Solid line and closed circles denote the clean simulations (N_a = 100 cm^{-3}), and the dashed line and diamonds represent the polluted simulations (N_a = 1000 cm^{-3}). Note the strong, and sometimes dominant contributions of small clouds to reflectance.

significant numbers of small clouds. The effect of aerosol on *n(a)* is reflected in the total number of detected clouds, which is higher in the polluted simulations; the fine resolution has 9738 polluted clouds and 8147 clean clouds. The number of clouds decreases with decreasing resolution because of the negative power-law size distribution.

Although more and more small clouds are resolved at the fine resolution, the slopes of the power-law fit do not differ significantly and are in good agreement with observations (*Koren et al.*, 2008) for small trade cumulus clouds at various locations. The slope of these cloud size distributions is important because it has a strong bearing on the relative contribution of small versus large clouds to cloud fraction and reflectance (Jiang et al., 2009).

Figure 1b shows the distribution of the normalized total reflectance, *R* as a function of cloud area *a*. The distributions are normalized such that the contribution from the smallest clouds is unity. This normalization highlights the *relative* contributions of different cloud sizes to *R*. For the polluted simulations, the smallest clouds contribute the most to reflectance. For the clean simulations, the distribution has a relatively flat form over a large range of cloud sizes. The strong (or dominant) contribution of the smallest clouds to *R* is consistent with observations (Koren et al., 2008). These analyses point to the important contributions that small clouds make to cloud reflectance, in addition to their relatively well known contributions to cloud fraction and number.

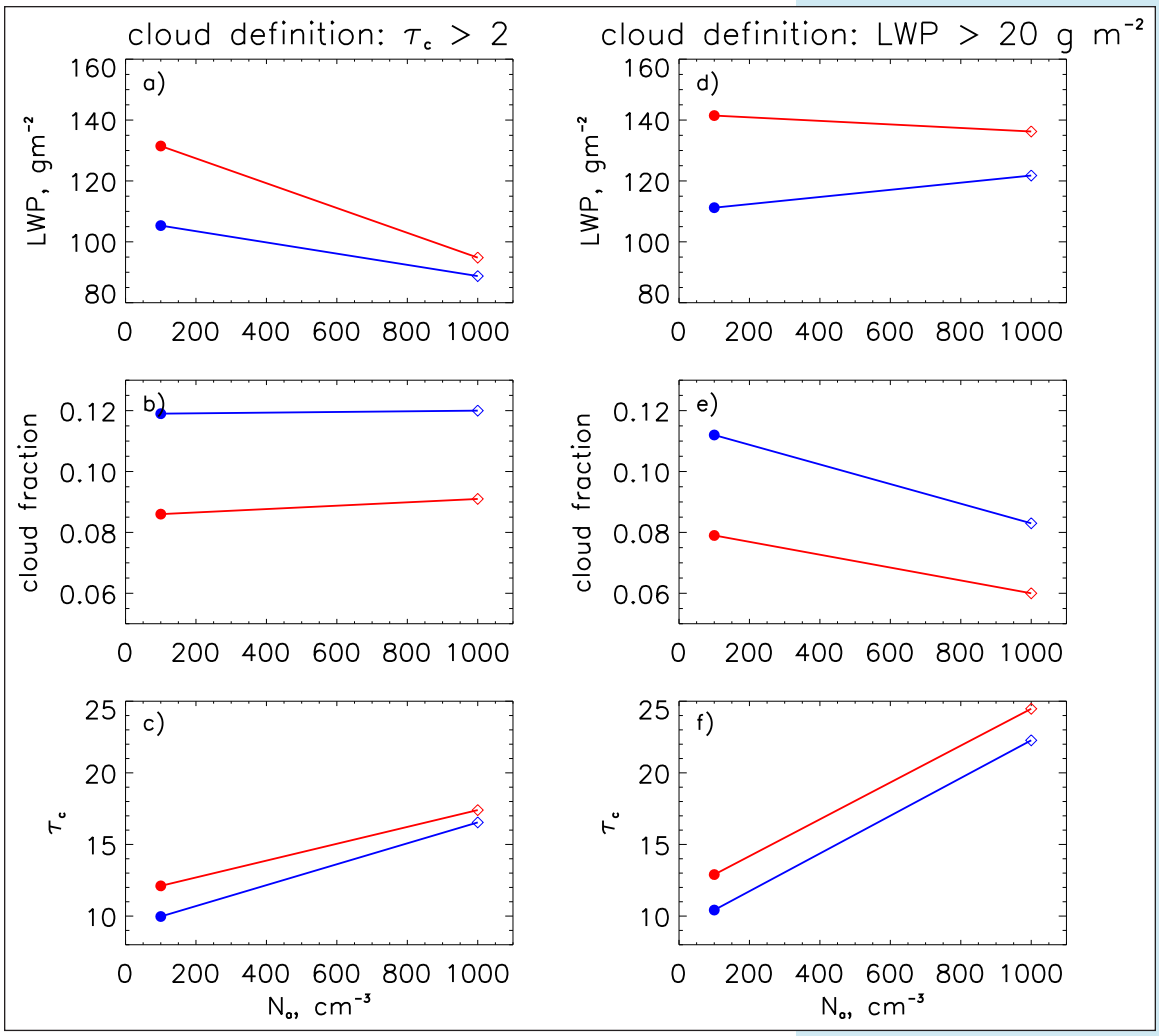

Figure 2. a) LWP averaged over cloudy columns, b) cloud fraction, and c) cloud optical depth τ_c averaged over regions with τ_c > 2 (left panel) and with LWP > 20 g m^{-2} (right panel). Blue denotes the fine resolution ($\Delta_{x,y}$ = 25 m, Δ_z = 10 m,), and red denotes the coarse resolution ($\Delta_{x,y}$ = 100 m, Δ_z = 40 m,). Note that responses of cloud fields to changes in aerosol depend strongly on the definition of "cloud."

The fact that these small clouds exist down to the smallest resolvable scales of our model means that larger-scale models may significantly underestimate contributions from shallow cumulus to these climatically important parameters.

Cloud Macroscale Properties

Cloudy regions can be defined based on somewhat arbitrary threshold values for LWP (> 20 g m^{-2}) or cloud optical depth τ_c (> 2). Both definitions have been used widely. However, the response of the cloudy-column-averaged LWP, *cf* (the ratio of cloudy columns to the total number of columns in the domain), and τ_c shows significant sensitivity to the cloud definition (Figure 2).

CUMULUS CLOUDS

For both cloudy column criteria, cloud fraction is significantly higher (~30%) at the fine resolution compared to the coarse resolution simulations because many smaller clouds are resolved by the fine resolution simulations. At any given resolution, cloud fraction based on $\tau_c > 2$ is always higher than that based on LWP > 20 g m^{-2}. Closer examination of the cloud fields indicates that this is because the τ_c criterion includes more small clouds than the LWP criterion.

It should be noted that the decrease in cloud fraction with decreasing model resolution results from the fact that as resolution decreases, the smallest clouds which contribute significantly to cloud fraction, are not resolved.

When $\tau_c > 2$ is selected to define a cloudy column (fig. 2 left panel), an increase in aerosol concentration N_a has little effect on cloud fraction, whereas LWP decreases significantly. When the LWP > 20 g m^{-2} criterion is used (fig.2 right panel), cloud fraction decreases by up to 26%, but LWP remains nearly constant in response to the increase in N_a. These differences in trends suggest that caution be exercised before drawing conclusions about cloud responses to aerosol perturbations. This is further underscored by the fact that LWP increases with increasing aerosol in the fine resolution simulations (Fig. 2d, blue) and decreases in the coarse resolution (Fig. 2d, red).

The response of τ_c to a change in aerosol is well-captured at all resolutions for a given "cloudy" definition; however the degree of this increase (akin to the albedo susceptibility dA/dN_d of the clouds) depends quite strongly on the τ_c criterion.

The above results suggest that the resolution of the simulation significantly affects the absolute values of commonly used metrics of cloud macrophysical properties. Which definition of "cloud" should be chosen is highly dependent on the application. For example, the choice of the optical depth threshold of $\tau_c > 0.5$ is more appropriate when considering the albedo continuum from aerosol (in various states of humidification) to cloud.

Concluding Remarks

Small clouds contribute significantly to cloud fraction and reflectance and therefore need to be taken into account in climate studies. Aerosol perturbations to small cumulus cloud fields tend to generate more small clouds, likely as a result of enhanced evaporation of smaller drops at cloud edge.

This study supports a growing body of research that although precipitation suppression by aerosol appears to be robust, aerosol may affect shallow cumulus clouds in ways other than the commonly assumed enhancements in LWP and cloud fraction enhancement associated with the "second indirect effect". The responses could depend on the definition of "cloud". Care should be taken before assuming that the responses in LWP and cloud fraction always act in accord with this simple construct.

References

Feingold, G., S. M. Kreidenweis, B. Stevens, and W. R. Cotton, 1996: Numerical simulation of stratocumulus processing of cloud condensation nuclei through collision-coalescence. *J. Geophys. Res.*, 101, 21,391 - 21,402.

Jiang, H., G. Feingold, and I. Koren, 2009: Effect of aerosol on cumulus cloud morphology. Submitted to *J. Geophys. Res.*

Koren, I, L. Oreopoulos, G. Feingold, L. A. Remer, and O. Altaratz, 2008: How small is a small cloud. *Atmos. Chem. Phys.*, 8, 3855 - 3864.

Plank, V. G., 1969: The size distribution of cumulus cloud in representative Florida populations. *J. Appl. Meteor.*, 8, 46-67.

Rauber, R. M., and co-authors, 2007: Rain in shallow cumulus over the ocean, the RICO campaign. *Bull. Amer. Meteor. Soc.*, 88, 1727-1738.

NNEW

NextGen Network Enabled Weather (NNEW) Program

Chris MacDermaid and MarySue Schultz

CIRA researchers at NOAA's Earth System Research Laboratory (ESRL) Global Systems Division (GSD) are playing a key role in developing the capability to provide weather information to tomorrow's aviation system using state-of-the-art technology. Funding for this work is provided by the Federal Aviation Administration (FAA) as part of the Next Generation Air Transportation System (NextGen), a Congressionally-mandated (Vision 100 – Century of Aviation Reauthorization Act, December 2003) multi-agency and public-private initiative.

"NextGen is focusing on a new direction in aviation weather-information capabilities to help stakeholders at all levels make better decisions during weather situations. Safe and efficient NextGen operations will be dependent on enhanced weather capabilities based on three major tenets:

- A common picture of the weather for all aviation decision makers and aviations system users
- Weather integrated directly into sophisticated decision-support capabilities to assist decision makers
- Utilization of Internet-like information dissemination to realize flexible and cost-efficient access to all necessary weather information."[1]

The NextGen Network Enabled Weather program (NNEW) "... will serve as the core of the NextGen weather support services and provide a common weather picture across the national airspace system. These services will, in turn, be integrated into other key components of NextGen required to enable better air transportation decision-making."[2]

"NNEW provides network access to weather information from distributed weather information sources (e.g., General Weather Processor) by all users, and fusion and integration of weather information into NextGen decision support systems. It is anticipated that tens of thousands of global weather observations and sensor reports from ground-, airborne-, and space-based sources would fuse into a single national weather information system, updated as needed in real-time."[3]

The NNEW program is responsible for defining the standards and providing the FAA's portion of the interagency infrastructure known as the 4-Dimensional Weather Data Cube (4-D Weather Data Cube). The 4-D Weather Data Cube will provide standards-based access to aviation weather data. Users of the 4-D Weather Data Cube will have improved access to timely and accurate weather information to support improved decision making, while enhancing aviation safety. The 4-D Weather Data Cube will comprise weather data held in various distributed databases within the FAA, the National Oceanic and Atmospheric Administration (NOAA), and the Department of Defense (DoD), as well as commercial weather databases. The 4-D Weather Data Cube will also include the registries and repositories needed for data discovery and access, as well as provide the capability to mediate among the various standards that will be employed and will provide the capability to support retrieval requests such as along a flight trajectory.

CIRA researchers at ESRL GSD are collaborating with researchers at the Massachusetts Institute of Technology's Lincoln Laboratory (MIT/LL) and at the National Center for Atmospheric Research's Research Applications Laboratory (NCAR/RAL) on NNEW. MIT/LL is primarily responsible for the registry/repository, NCAR/RAL is primarily responsible for the gridded weather data server, and ESRL GSD is primarily responsible for the non-gridded weather data server, which is based on the Web Feature Service (WFS) standards defined by the Open Geospatial Consortium (OGC). ESRL GSD is also responsible for performance testing in collaboration with the FAA's William J. Hughes Technical Center (WJHTC), which serves as the systems test base for the FAA. The three laboratories are working together on data modeling, with ESRL GSD providing technical oversight. The CIRA researchers involved with this program are Chris MacDermaid (technical lead), MarySue Schultz,

[1] *Four Dimensional Weather Functional Requirements for NextGen Air Traffic Management* version 0.1 July 18, 2008

[2] *Operational Evaluation Partnership Plan Reference Sheet NNEW*, July 19, 2007

[3] *Operational Evaluation Partnership Plan Reference Sheet NNEW*, July 19, 2007

NNEW

James Frimel, Paul Hamer, Patrick Hildreth, and Glen Pankow.

Web Feature Service

Background

The OGC is a non-profit, international, voluntary consensus standards organization that is leading the development of standards for geospatial and location based services. The OGC is a consortium of private sector companies, government agencies and universities participating in a consensus process to develop publicly available interface specifications. The specifications enable technology developers to make complex spatial information and services accessible to a variety of applications, and enable geo-processing technologies to interoperate or "plug and play".[4] The OGC is in the process of developing standards for a Web Coverage Service (WCS), Web Feature Service (WFS), and Web Map Service (WMS).

The WFS standard defines interfaces and operations for data access and manipulation of geographic features across the Web using platform-independent calls. The basic WFS allows querying and retrieval of features. A transactional WFS (WFS-T) additionally allows creation, deletion, and updating of features. The WFS returns geospatial objects in Geography Markup Language (GML). GML is an eXtensible Markup Language (XML) dialect which can be used for modeling geographic features, and for passing data back and forth between a WFS and a client. WFS implementations can also use other formats for transport, but GML must be supported. Currently, WFS version 1.0.0 and version 1.1.0 are available for public use. WFS version 1.0.0 requires the use of GML version 2.1.2, and WFS version 1.1.0 requires GML 3.1.1.

The NNEW project has elected to implement the WFS standard for accessing non-gridded data, and will build a reference implementation of the WFS standard (WFS-RI). The WFS-RI will demonstrate the WFS standards as they apply to NextGen's weather data access needs, and will eventually become operational, providing access to data from the 4-D Weather Data Cube for all FAA users. The NNEW WFS-RI will initially supply point data (METARs, PIREPs, MDCRS, etc.) and Nexrad Level III overlay products (such as Storm Structure, Hail Index, Storm Tracking, etc.); eventually features such as gust fronts and icing forecasts derived from model output data will be added.

Development Process

ESRL GSD and CIRA are responsible for developing the WFS-RI. The development process has three stages:

1. Defining user and system requirements for the WFS. ESRL GSD and CIRA collaborated with NCAR/RAL and MIT/LL to define the system requirements (for example: what level of security is provided, which operating systems are supported). The user requirements are being collected by the FAA, and have only been defined at a high-level at this point. The requirements will be documented, and will be used for designing and implementing the WFS-RI, to make sure FAA users are provided with all necessary functionality.
2. Investigating WFS implementation options. Three options have been identified for developing the WFS-RI:
   - Leverage existing open source implementations
   - Purchase a commercial package
   - Build the reference implementation in-house

   The ESRL GSD/CIRA team will evaluate each option, compare them, and select the one that best satisfies FAA requirements.
3. Rapid prototype development and testing. After the best implementation option has been selected, a cycle of design, development, and user testing will be initiated. To start, the developers will create a prototype WFS that has a few basic capabilities. FAA users will be invited to exercise and evaluate the prototype and provide feedback. Input from the users will be incorporated into the next cycle. This process ensures that user requirements are being met, and lowers the risk that the final system will not be adequate for operational use. The rapid prototype phase will produce

[4] Paraphrased from the OGC Web Site

a WFS implementation that will be installed for testing in the field.

Progress

During 2008, the WFS team investigated the first implementation option: existing open source systems. This option is attractive because open source code can be customized and extended, and the software is available without costly licensing. The capabilities of three open source WFS's (GeoServer, MapServer and Degree) were compared. GeoServer had a few advantages over the others: 1) it is a servlet, which has significantly less overhead and runs faster; 2) it uses GeoTools, a Java code library which makes modifications and customizations more accessible; and 3) it has a web interface that makes initial set-up faster. GeoServer was selected for further experimentation. ESRL GSD and CIRA developed a prototype WFS using GeoServer and the PostgreSQL database that distributed METAR and PIREP data, and demonstrated these capabilities to FAA management in the fall of 2008. Some problems with GeoServer were encountered during the prototyping exercise, which emphasized the need to investigate the other options: building the WFS-RI in-house and purchasing a commercial package.[5]

The investigation of commercial solutions will be conducted in 2009. The WFS development team has identified four vendors as good candidates: IBM/Informix, Oracle, CubeWerx, and ERDAS/RedSpider. Each of these vendors has a WFS/database package that appears to be mature enough to provide the necessary capabilities. The vendors have been in existence long enough not to be high-risk. The development team has interviewed all of the vendors, and obtained information pertaining to how their WFS implementations satisfy FAA requirements. The development team is currently in the process of evaluating this information, and will decide whether to experiment further with any of the vendor implementations.

The final option, building the WFS-RI in-house, will also be evaluated in 2009. We will need to produce development cost and time estimates, in order to compare this option with the others.

Data Modeling

Background

The FAA, DoD, and the National Weather Service (NWS) are working with the European Organization for the Safety of Air Navigation (EUROCONTROL) on a Weather Information Data Exchange Model (WXXM) based on XML. This will be compliant with the OGC's GML specifications.

Progress

A WXXM workshop was held in Washington, D.C. the week of November 10, 2008. The outcome of the workshop was an agreement between the FAA and EUROCONTROL to jointly develop future versions of Weather Information Models. The NNEW program has responsibility for creating the candidate version 1.1 of the WXXM.

Performance Testing

Background

For the NNEW project to be a success, it must be clearly demonstrated that the FAA requirements for timely receipt of aviation weather data are met and that all aviation weather data users have a common weather picture. GSD is working with the WJHTC to capture current FAA end user/system requirements for aviation weather data and document the transition of these requirements to future FAA weather needs in a form that can be used to help in validation testing of the NNEW aviation weather data discovery/delivery protocols.

The GSD performance testing tool created for this testing, called the NNEW Evaluation Weather Tool (NEWT), will allow for testing the NNEW discovery/delivery from a real-use perspective, such as the Enhanced Traffic Management System (ETMS) implemented at FAA Traffic Management Units. The NEWT is easily configurable to receive all ETMS or other FAA system data for testing and can be easily installed at multiple sites/systems so that a true load can be put on the NNEW services for particular classes of users. The NEWT system can be viewed as a risk reduction system not only for NNEW

[5] GeoServer handles time asymmetrically. Time fields in the request must be in the format used by the database, while time fields in the reply are in ISO8601 format. Also, although it was possible to modify the code, there was quite a bit of time required to understand the architecture and build environment. GeoServer developers were helpful with these issues, but it sometimes took several days for them to respond to questions.

NNEW

specification/implementation but for architecture design/implementation.

Progress

The NEWT in 2008 demonstrated the following NNEW testing capabilities:

1. Black box testing capabilities for the NNEW OGC WFS and WCS interfaces
   a. Specification implementation
   b. Specifications assessment
2. Performance testing between old methods of receiving weather data and NNEW
   a. When are the data available for use?
   b. Where are the bottlenecks?
   c. How does it compare to current delivery systems?
3. Risk Reduction
   a. Document specification/implementation concerns
   b. Work with developers to resolve problems
   c. Retest

Demonstrations

Description

NNEW is using a phased software development process. Until now, each year's activities have included research and prototyping. At the end of each fiscal year, new capabilities are formally tested, and demonstrated to NNEW management at the WJHTC.

Phase I

Phase 1 of the NNEW project (2006-2007) involved exploring OGC gridded data services and static cataloging. Each of the partner labs developed a WCS capability that exposed gridded data available at their facilities, and MIT/LL also developed an initial catalog server. A demonstration of the WCS servers and the catalog server was given to FAA management in December, 2007. GSD used Unidata's WCS (THREDDS) to provide access to the Meteorological Assimilation Data Ingest System (MADIS) Rapid Update Cycle (RUC) Surface Assimilation System (RSAS) data. NCAR/RAL provided WCS access to their Aviation Digital Data Service (ADDS) database, and MIT/LL provided WCS access to Corridor Integrated Weather System (CIWS) data. The demonstration showed the ease with which distributed OGC servers can be accessed. A single client, based on the ADDS flight path tool developed by NCAR/RAL, accessed all three WCS servers and the catalog server. Different versions of the WCS standard were implemented at the different sites. The Phase I demonstration system architecture is shown in Figure 1.

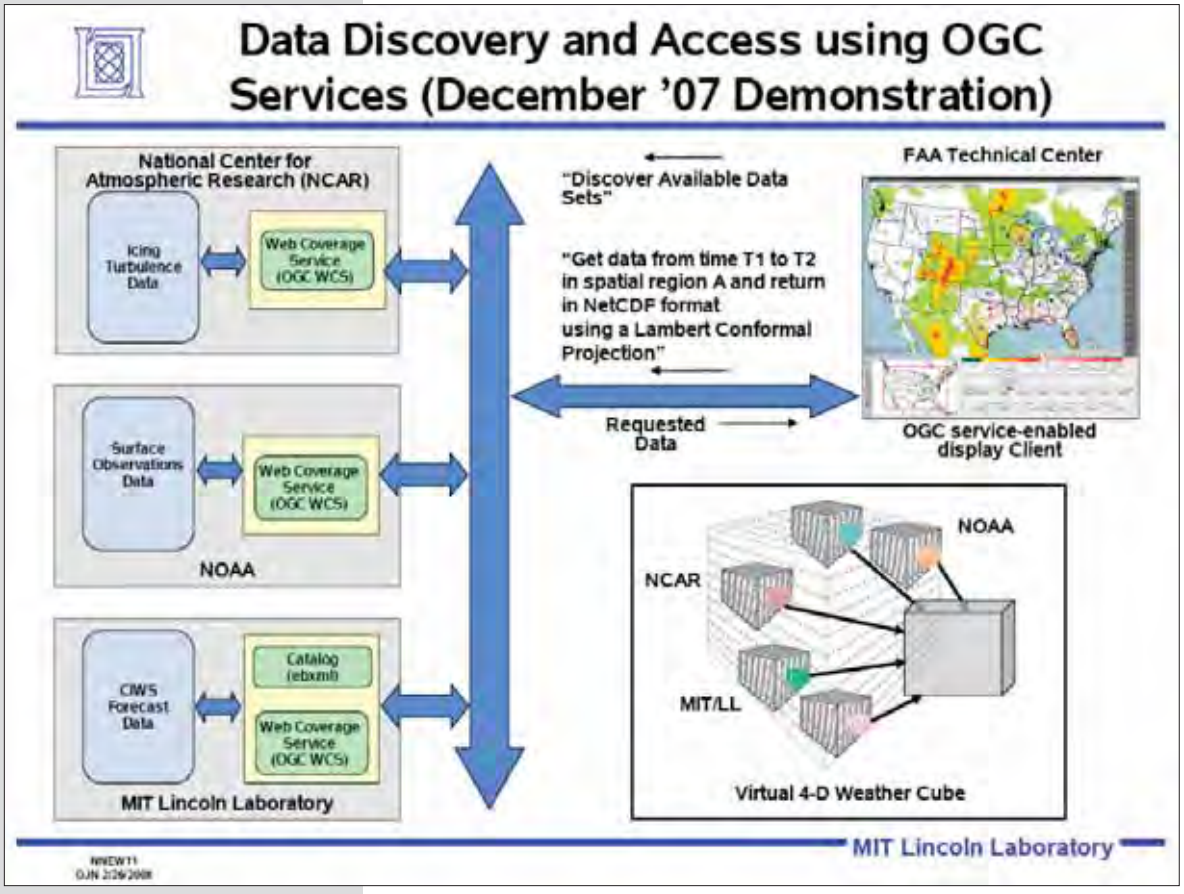

Figure 1. 2007 Demonstration System

Phase II

For Phase II (2008), the development labs expanded their research to include WFS capabilities, in particular open source implementations of the WFS standard. As described above, GeoServer was selected for further experimentation, and NCAR/RAL and ESRL GSD both developed WFS capabilities using GeoServer. The testing and demonstrations at the end of 2008 involved both of these WFS servers, as well as the WCS and catalog servers developed the previous year. There were two clients involved: the NCAR/RAL client used the previous year and NEWT. The NCAR/RAL client retrieved and displayed data from the servers of NCAR/RAL, MIT/LL and GSD. NEWT accessed and displayed data from MIT/LL's WCS and from ESRL GSD's WFS. The Phase II demonstration system architecture is shown in Figure 2. As in the previous year, the demonstrations illustrated the distributed database concept, with each lab accessing data and information from the others. In addition, the 2008 testing included some performance tests, which will become increasingly important as development continues.

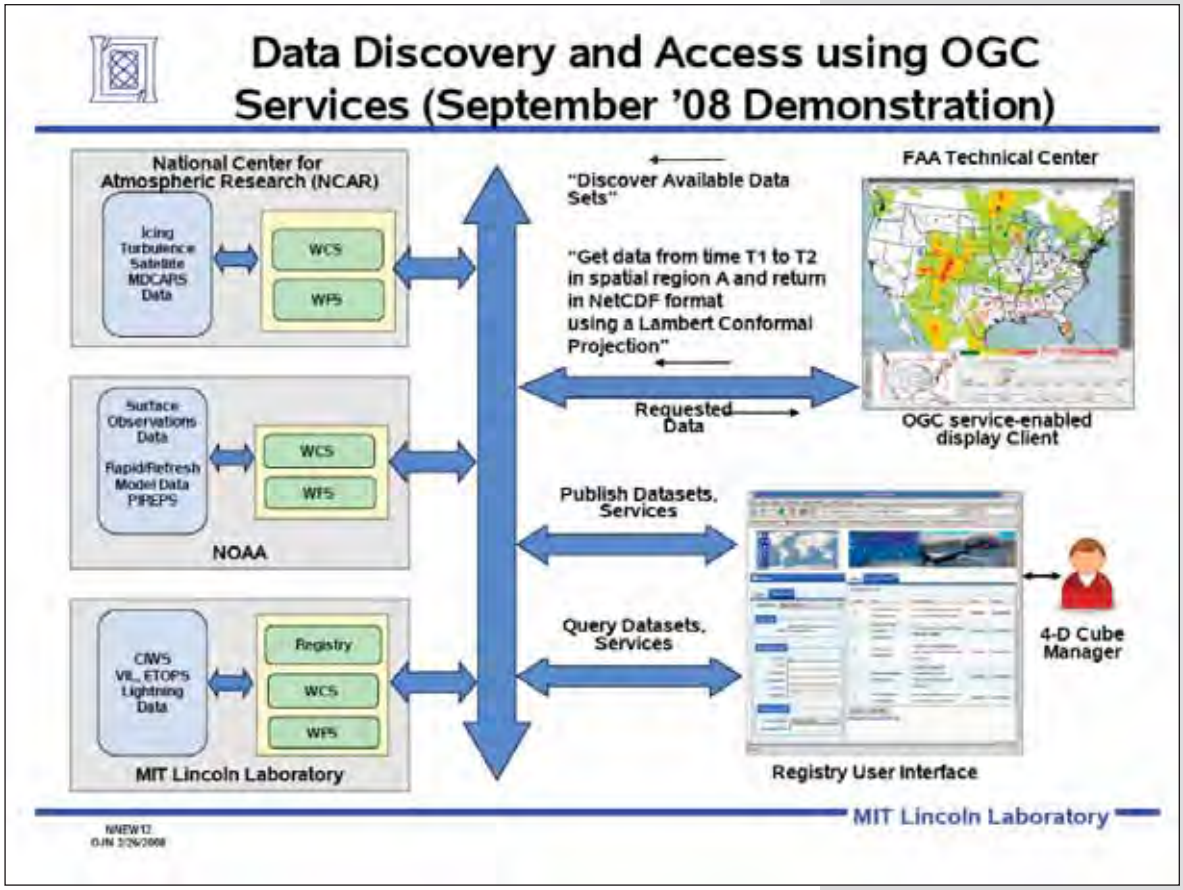

Figure 2. 2008 Demonstration System

Future Plans

In 2009, the WFS team will select the implementation option that best satisfies FAA requirements. After this is done, development of the WFS-RI will begin. Between 2009 and 2012, capabilities will gradually be added to the WFS-RI, and these will be tested and demonstrated at the WJHTC. In 2013, the WFS-RI will be installed in the field for testing by operational FAA sites. The NNEW project is scheduled to continue until 2025, when the 4-D Weather Data Cube and the associated data access services (such as the WFS-RI) will be installed operationally. End-to-end system testing, performance testing, and moving the systems into operations will become increasingly important between 2013 and 2025. ESRL GSD and CIRA will continue to be involved in the research, development, and testing needed to make the NNEW project a success.

HURRICANE FORECASTS

Exploring How Improved Hurricane Forecasts Can Benefit Society

Andrea Schumacher, Mark DeMaria (NOAA/NESDIS) and John Knaff (NOAA/NESDIS)

Figure 1. The Monte Carlo wind speed product probabilities for hurricane force (64 kt) winds, Hurricane Ike at 7pm CDT on 10 September 2008.

Figure 2. The total hurricane warning distances for the official NHC warnings and the objective scheme-derived warnings (MC Prob) for all sample set hurricanes, 2004-2008.

Over the last five years (2004-2008), 10 hurricanes have made landfall along the U.S. mainland, resulting in more than 1,600 deaths and close to $170 billion in damages in the U.S. alone. These recent, immense losses have highlighted the need for improvements in tropical cyclone forecasting and how society prepares for and responds to hurricanes. As the official national source of tropical cyclone forecasts, the National Oceanographic and Atmospheric Association (NOAA) has made improving tropical cyclone track, intensity, and storm surge forecasts a high priority.

Scientists at the Cooperative Institute for Research in the Atmosphere (CIRA) have a long history of research in tropical cyclones, with an emphasis on developing forecast guidance products. Many of these products, such as the National Hurricane Center (NHC) Tropical Cyclone Wind Speed Probability product (DeMaria et al. 2009) and the NESDIS Tropical Cyclone Formation Probability product (Schumacher et al. 2009), have been transitioned to operational products used routinely by tropical cyclone forecast agencies around the world.

It is generally accepted that improvements to hurricane forecasts will benefit society. Longer lead times will allow people more time to adequately prepare. Better track and structure forecasts could lead to more precise hurricane warning areas, which may reduce the costs of unnecessary evacuations. Quantifying these benefits, however, is a difficult task. How much money will a given forecast improvement save us? How many lives will be saved? These are tough questions to answer, but a new project underway at CIRA provides hope for making direct connections between forecast improvements and socioeconomic factors.

This project involves two main steps; 1) develop an objective scheme that simulates official hurricane warnings based on real-time hurricane track and intensity forecasts and 2) use this objective scheme to determine the changes in warning length and duration that result from artificially "improving" the real-time track and intensity forecasts. Since hurricane warnings are related to official hurricane evacuation orders, diagnosing potential reductions in coastal distance or duration of hurricane warnings can then be connected to reductions in unnecessary evacuations and their corresponding costs.

First, an objective hurricane warning scheme was developed using the Monte Carlo

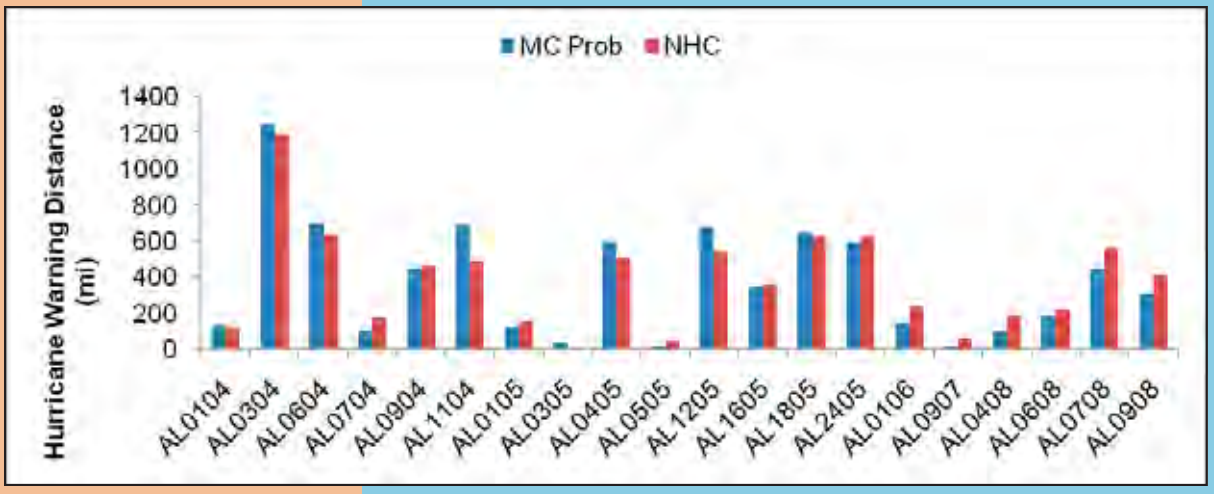

(MC) wind speed probability model. The MC model was developed by Regional and Mesoscale Meteorology Branch (RAMMB) scientists at CIRA, and an operational version* has been used by the NHC since 2006. The MC model uses a random sampling method, known as the Monte Carlo method, to account for errors in track, intensity, and structure from official forecasts over the last five years. It uses these sampled errors, along with the current official forecast, to generate 1,000 forecast realizations from which probabilities are derived. Both incremental and cumulative probabilities of 34-kt, 50-kt, and 64-kt winds occurring at a location within 0, 12,…, 120 hours are generated. Probabilities are computed every six hours and are displayed as contour plots on the NHC website (Fig 1). The MC model's dependence on both track and intensity forecasts as well as the forecast errors make it ideal for use in this project.

As expected, the MC model probabilities were found to be well correlated with the issuance of official hurricane warnings for U.S. landfalling hurricanes from 2004-2008. It was found that using a threshold of p>8% to issue a hurricane warning and p=0% to take a warning down produced warnings whose coastal lengths and durations were very similar to the NHC warnings (Fig. 2). Examples of the objective scheme warnings compared to the official NHC warnings for Hurricanes Gustav and Ike are shown in Figs. 3 and 4, respectively.

The second step of this analysis involved artificially reducing the track and intensity errors in the forecasts used to create the wind speed probabilities in the MC model. Since the observed tracks and intensities for the sample set hurricanes from 2004-2008 are archived by the Automated Tropical Cyclone Forecast System (ATCF, Sampson and Schrader 2000), artificially "improving" the input forecasts involved little more than adjusting the input forecasts closer to the observed values and scaling the errors sampled by the MC model. For this study, adjustments were made to the MC model reflecting 20% and 50% reductions in forecast track and intensity errors.

The objective hurricane warning scheme was then applied to this new set of wind speed probabilities, yielding new simulated hurricane warnings. Comparing these new warnings, which represent the warnings that potentially would have been issued for the sample hurricanes if the forecasts had been improved by 20% and 50%, to the control warnings reveals changes in length of

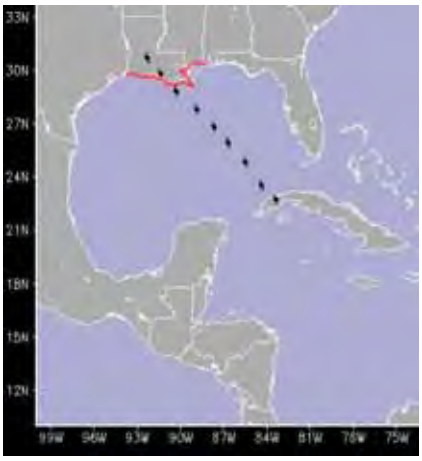

Figure 3. Official NHC issued warnings (left) and objective scheme warnings (right) for Hurricane Gustav (2008).

Figure 4. Official NHC issued warnings (left) and objective scheme warnings (right) for Hurricane Ike (2008).

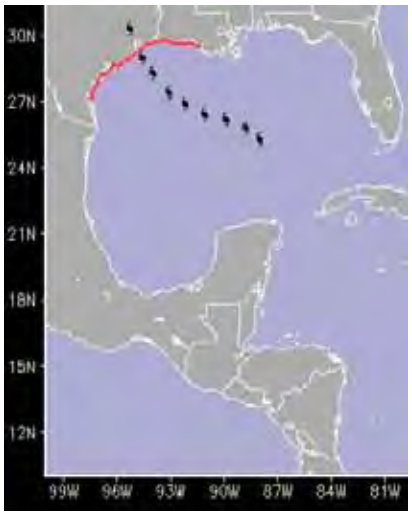

* More information on the NHC Tropical Cyclone Wind Speed Probability Products can be found at http://www.nhc.noaa.gov/aboutnhcprobs2.shtml

HURRICANE FORECASTS

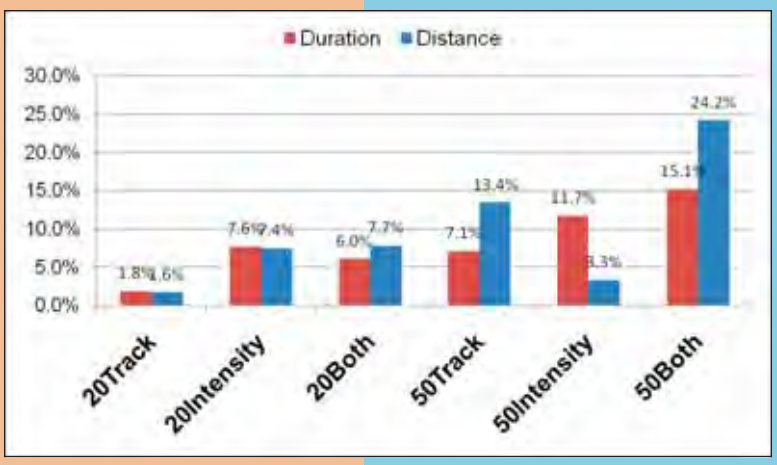

Figure 5. Resulting reductions in warning duration (red) and coastal length (blue) resulting from 20% error reductions in track (20Track), intensity (20Intensity), and both track and intensity (20Both) and 50% error reductions in track (50Track), intensity (50Intensity), and both track and intensity (50Both).

Figure 6. Objective scheme generated hurricane warnings for Hurricane Gustav (2008) after 20% (left) and 50% (right) reductions in forecast track and intensity errors. The red lines indicate warning areas that did not change with forecast error reductions and the blue lines indicates areas that were removed from the warning area when forecast error was reduced.

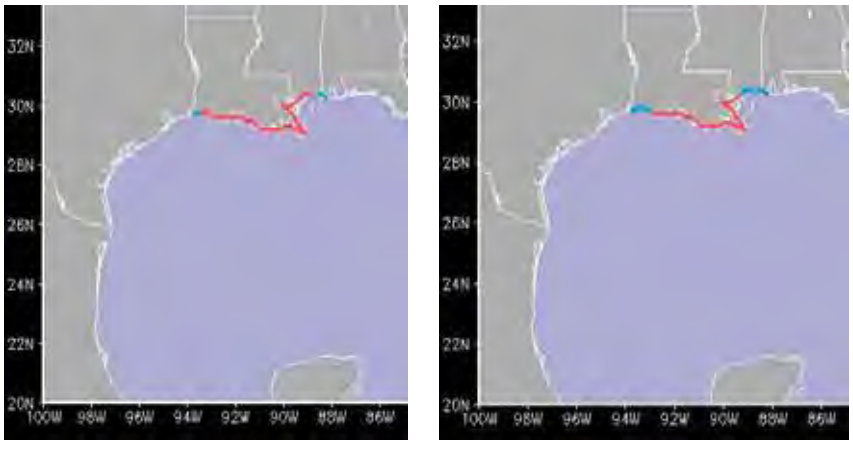

coastline warned and the amount of time warnings lasted. Results of this analysis suggest that a 20% reduction in hurricane forecast track and intensity errors results in a 29 mile (7.7%) reduction in the amount of coastline unnecessarily warned and lets the warning be dropped 2h (6.0%) sooner (Fig. 5). Similarly, a 50% reduction leads to a 92 mile (24.2%) reduction in the amount of coastline unnecessarily warned and lets the warning be dropped 5 h (15.1%) sooner.

Although reductions in the size of hurricane warnings (i.e., area that is over-warned and the time a warning is kept up after the threat has passed) should be directly relatable to a reduction in the costs of hurricane warnings to society, work is still underway to determine the most relevant relationship. Previous studies have suggested that household evacuation behavior is influenced by the receipt of an official order to evacuate (e.g., Baker 1991), and that official hurricane warnings are used by emergency managers to guide the issuance of evacuation orders. However, there are numerous other factors that influence the evacuation behavior of individuals, making defining a relationship between hurricane warnings, evacuation response, and hence evacuation costs a challenging task. Previous NHC publications have estimated the cost of an evacuation to be roughly $600,000 per coastal mile (Jarell and DeMaria 1999). A recent study has shown that this estimate may be too high, and at the very least does not take into account sharp difference in population density along the U.S. coast (Whitehead 2003). In the coming months, scientists plan to conduct individual storm analyses to construct case-specific estimates of socioeconomic savings resulting from the scheme-derived warning reductions (see Fig. 6). With this information, we will be given the rare opportunity to see what a future scenario for improved hurricane forecasting might actually look like, and more importantly what these improvements will mean for the society scientists serve.

References

Baker, Earl J., 1991. Hurricane Evacuation Behavior. *International Journal of Mass Emergencies and Disasters* 9: 287-310.

DeMaria, M., J. A. Knaff, R. Knabb, C. Lauer, C. R. Sampson, R. T. DeMaria, 2009: A New Method for Estimating Tropical Cyclone Wind Speed Probabilities. *Wea. Forecasting*, Submitted.

Jarell, J.D. and M. DeMaria, 1999. An Examination of Strategies to Reduce the Size of Hurricane Warning Areas. 23rd Conference on Hurricanes and Tropical Meteorology, Dallas, TX, 10-15 January 1999.

Sampson, C. R. and A. J. Schrader, 2000: The automated tropical cyclone forecasting system (Version 3.2). *Bull. Amer. Met. Soc.*, 81, 1231-1240.

Schumacher A.B., DeMaria M., Knaff J.A. (2008) Objective Estimation of the 24-Hour Probability of Tropical Cyclone Formation. *Weather and Forecasting*: In Press.

Whitehead, J.C., 2003: One million dollars per mile? The opportunity costs of Hurricane evacuation. *Ocean and Coastal Management*, 46, 1069-1083.

CIRA COMMUNIQUÉ

Night Sky Program Featured in *Fort Collins: Now*

An excerpt from the January 15th issue follows:

"On an especially clear night, like the evening the National Park Service's dark sky guru measured Fort Collins' dark sky pulse, the sky is inkier than may be expected in a city. But it's not dark enough for people like Chad Moore. He directs the park service's Night Sky Program, spending much of our sleeping hours bundled in a parka, hovering over a laptop and camera, measuring how city lights mask the stars. Moore is well known among an army of researchers fighting to save the darkness. They believe the loss of dark skies is a threat to human and wildlife health, scientific knowledge, and the human spirit. Though light pollution is a growing environmental problem, it's one of the easiest to reverse.

Steve Koch Becomes Fellow of AMS

The American Meteorological Society announced that Steven E. Koch, director of the Global Systems Division at the National Oceanic and Atmospheric Administration's Earth System Research Laboratory in Boulder, has become a fellow of the society. Koch is a CIRA Fellow and member of the CIRA Advisory Council. Koch's area of expertise is in numerical weather prediction, data assimilation, predicting turbulence, and understanding large-scale meteorological events.

Frank Kelly Named Director of the Alaska Region at NWS

Dr. Frank P. Kelly assumed responsibilities as Regional Director for the Alaska Region at the National Weather Service (NWS) on October 27, 2008. In this position, Dr. Kelly oversees the management of all operational and scientific meteorological, hydrologic, and oceanographic programs of the region including observing networks, weather services, forecasting, climatology, and hydrology. Prior to assuming this position, Dr. Kelly served as the head of the Programs and Plans Division of the Office of Science and Technology at NWS since 2002. His education includes both master's and doctoral degrees in atmospheric science from Colorado State University and a bachelor's in earth science from Montana State University.

January 2009 GSD Team Member of the Month – Jim Ramer

The following nomination comes from Information Systems Branch Chief Carl Bullock.

"Jim has been an extremely productive member of ISB providing much of the display functionality of AWIPS, including the improvements allowing NWS to move to storm based warnings this past year.

More recently, Jim has developed tools to allow forecasters to explore model ensemble data in an innovative way.

Jim has also played a key role in getting the data flowing to the Hydrometeorological Testbed systems for the winter experiment."

February 2009 GSD Team Member of the Month – Tom Henderson

The following nomination comes, via Aviation Branch Chief Mike Kraus, from AB/Advanced Computing Section's Mark Govett.

"Tom Henderson is being recognized for his significant contributions in several critical areas – modeling frameworks, FIM software development, and the Scalable Modeling System (SMS) redesign. Modeling frameworks help NOAA and its collaborators more easily use and integrate their work into larger modeling systems such as ensembles, coupled models, and complex earth system models.

"Tom has also established a software infrastructure for the FIM model. He utilized both GForge and Subversion for software development, and built a testing infrastructure to ensure upgrades to FIM are tested. Since the FIM software repository has been established over nine months ago, there have been almost 500 commits by members of the FIM team. Tom also recently redesigned and modernized the Scalable Modeling System I/O capabilities to support the ability to efficiently run the 15km version of FIM on wjet and the TACC machines. Tom's work led to over 50,000 lines of code being removed from SMS."

2008 GSD Web Award ("Webbie") Winner – Brian Jamison

Best New Site – Brian Jamison for the FIM Real-Time Model Graphics Sites

These sites provide real-time images of FIM global model output for the entire globe and selected sub-regions such as the CONUS, Africa, the Arctic, and Atlantic and Pacific basins. These plots have been invaluable for making real-time images available to developers, both here at GSD and elsewhere. Brian's FIM graphics have been critical in showing that the FIM can be competitive with operational models for hurricane track forecasting. Check out Brian's sites.

- http://fim.noaa.gov/fimgfs/
- http://fim.noaa.gov/fimconusTACC/

ABBE Award for Robert Maddox

Former NSSL Director Robert Maddox, is honored for a lifetime of service to atmospheric science through seminal contributions to scientific research, inspirational leadership, and exemplary program management that promoted important interactions between research and operations. The Cleveland Abbe Award for Distinguished Service to Atmospheric Sciences by an Individual is presented on the basis of activities that have materially contributed to the progress of the atmospheric sciences or to the application of atmospheric sciences to general, social, economic, or humanitarian welfare.

Dr. Robert Maddox is internationally recognized as an expert on mesoscale cloud systems who has worked at the National Severe Storms Lab in Norman Oklahoma, and is now a professor at the University of Arizona. His characterizations of mesoscale convective complexes (MCCs) were pioneering. Dr. Maddox was a CIRA Ph.D. student in the late 1970s/early 1980s under Professor Thomas Vonder Haar.

CIRA Mission

The mission of the Institute is to conduct research in the atmospheric sciences of mutual benefit to NOAA, the University, the state, and the nation. The Institute strives to provide a center for cooperation in specified research program areas by scientists, staff, and students and to enhance the training of atmospheric scientists. Special effort is directed toward the transition of research results into practical applications in the weather and climate areas. In addition, multidisciplinary research programs are emphasized, and all university and NOAA organizational elements are invited to participate in CIRA's atmospheric research programs.

The Institute's research is concentrated in several theme areas that include global and regional climate, local and mesoscale weather forecasting and evaluation, applied cloud physics, applications of satellite observations, air quality and visibility, and societal and economic impacts, along with cross-cutting research areas of numerical modeling and education, training, and outreach. In addition to CIRA's relationship with NOAA, the National Park Service also has an ongoing cooperation in air quality and visibility research that involves scientists from numerous disciplines, and the Center for Geosciences/Atmospheric Research based at CIRA is a long-term program sponsored by the Department of Defense.

Cooperative Institute for Research in the Atmosphere

College of Engineering – Foothills Campus, Colorado State University
1375 Campus Delivery, Fort Collins, CO 80523-1375
(970) 491-8448

www.cira.colostate.edu

If you know of someone who would also like to receive the *CIRA Magazine*, or if there are corrections to your address, please notify us.

Colorado State University